Accepted Manuscript online: 2022-06-10 Article published online: 2022-06-29

Experimental and Computational Studies of Phenylene-Bridged Azaacenes as Affinity Materials for Sensing Using Quartz Crystal Microbalances

Ephraim Prantl[a]
Sebastian Hahn[b]
Uwe H. F. Bunz*[b]
Siegfried R. Waldvogel*[a]

[a] Department of Chemistry, Johannes Gutenberg University Mainz, Duesbergweg 10–14, 55128 Mainz, Germany
[b] Institute of Organic Chemistry, Ruprecht Karl University of Heidelberg, Im Neuenheimer Feld 270, 69120 Heidelberg, Germany
* Uwe.Bunz@oci.uni-heidelberg.de, waldvogel@uni-mainz.de

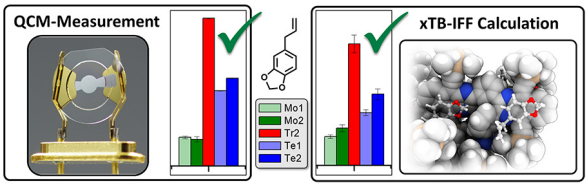

Received: 10. 05. 2022
Accepted after revision: 09. 06. 2022
DOI: 10.1055/a-1873-5186; Art ID: OM-2022-05-0004-OA

Abstract Phenylene-bridged, TIPS-alkynylated azaacenes are excellent materials for selective gas sorption. In this study, we utilized 195 MHz high-fundamental-frequency quartz crystal microbalances, coated with cyclic azaacenes, and determined their affinity towards hazardous and narcotics-related compounds such as benzene, γ-butyrolactone (GBL) or safrole. Computational investigations by extended tight binding intermolecular force field allowed better understanding of the determined unique features. Remarkable selective affinities were found towards GBL and safrole – both dangerous compounds which can be abused as precursors for narcotics. With these systematic approaches, we were able to get a better insight into the selective adsorption and how to design better affinity materials

Key words: affinity materials, quartz crystal microbalances, sensors, azaacene, trace analysis

Introduction

Selective and sensitive gas sensors and the increasing need to detect gas traces of hazardous, explosive, illicit and polluting chemicals are important challenges.[1,2] In particular, the abuse of compounds like amphetamines, γ-hydroxybutyric acid and their precursors phenylacetone, safrole, and γ-butyrolactone (GBL) has caused significant societal problems.[3,4] Furthermore, BTX (benzene, toluene and xylenes) analytes, used for example as rodenticides in overseas shipping containers, are hazardous for dockworkers if not detected beforehand.[5] Several approaches have been used so far with GC, GC-MS and ion mobility spectrometry (IMS). GC and GC-MS (GC–mass spectrometry) offer good detection capabilities but depending on the analyte they require derivatization and long acquisition times, and the required equipment is not easily portable.[6] IMS offers fast measuring times but a lack of selectivity and sensitivity.[7] Another promising approach is the use of transducers which facilitate affinity materials to selectively bind analyte of interest and therefore induce a signal on the transducer.[8,9] As transducer, excellent sensitivities can be found with quartz crystal microbalances (QCMs), Bragg sensors, microring resonators or cantilevers.[4,10–12] Highly sensitive and low-cost QCMs in combination with selective affinity materials create a powerful sensing system.[13,14] Installing these modified QCMs in an affordable mobile platform creates a new reliable sensor for in-field use with the potential to detect analytes within seconds.[13] However, designing and synthesizing selective affinity materials to find affordable commercial solutions for gas sensing is challenging.[9] Numerous affinity materials were investigated and showed quite unique behaviors.[2,4,12,15] A case with excellent selectivity, especially towards safrole, was reported for a microporous triptycene-based azaacene.[12] The combination of a rigid triptycene core providing high porosity and an azaacene moiety seemed to be crucial for this kind of selectivity.[16] This example was rather unique, as finding highly selective behavior proved to be very challenging and time consuming.[9] Therefore, it is of particular importance to find a theoretical model for the design of affinity materials to target specific analytes that can be used to determine and, in the best case, predict affinity trends. Dickert et al. used force field calculations (MM3) with some success.[17] More recently Grimme et al. employed extended tight binding intermolecular force field (xTB-IFF), which gave calculated data that fit well with experimental results.[18] With this computational method, 50 analytes were successively docked into a crystal structure of the affinity material and the respective single-point interaction ener-

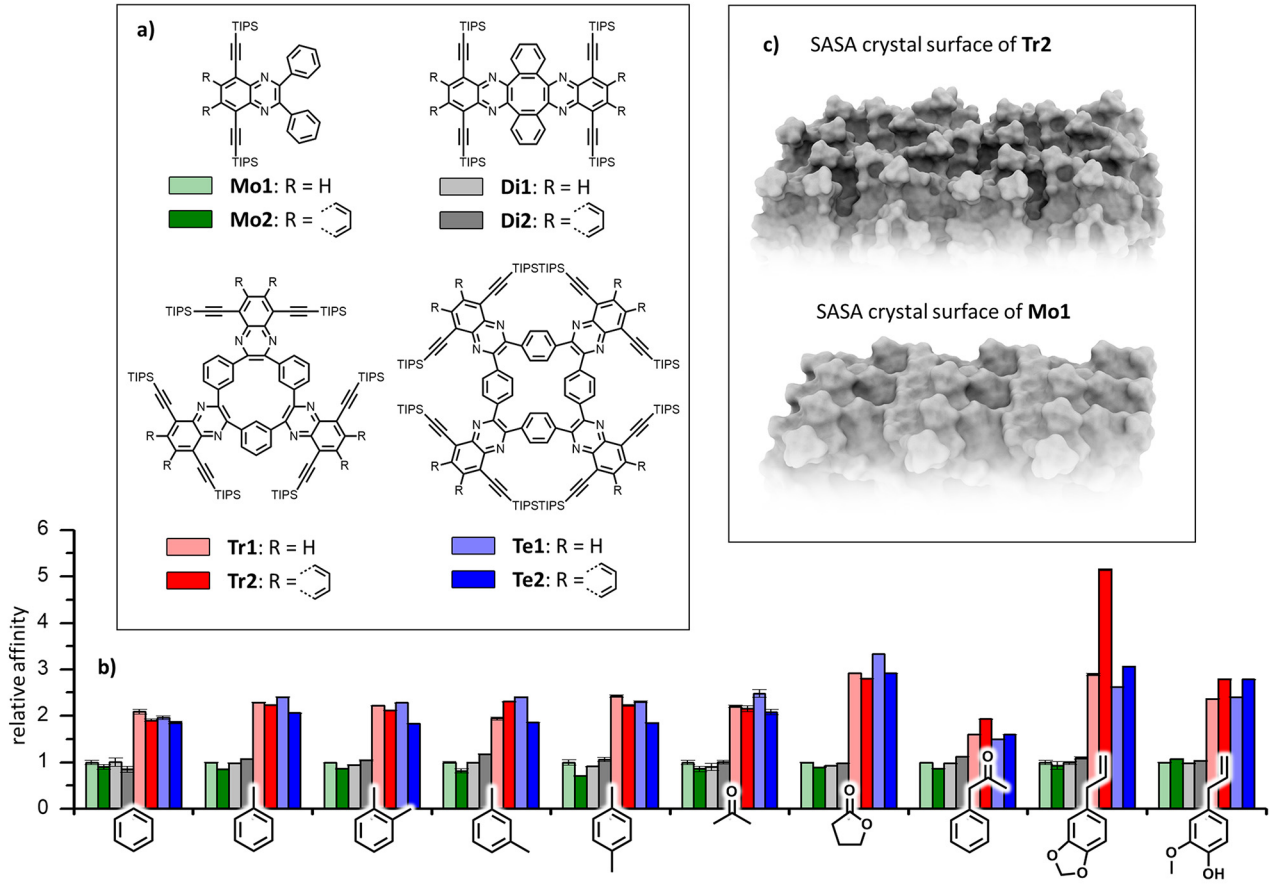

Figure 1 a) Phenylene-bridged azaacene affinity materials investigated by QCM measurements in a systematic approach. b) Determined affinities towards the analytes benzene, toluene, *o*-xylene, *m*-xylene, *p*-xylene, acetone, GBL, phenylacetone, safrole and eugenol normalized to **Mo1**. c) Display of the solvent-accessible surface area (SASA) by a probe radius of 1.4 Å of **Tr2** (top) and **Mo1** (bottom), created with Chimera X 1.3.[22,23]

gies were calculated, showing a similarity between QCM measurements and theoretical calculations for the first time.[18]

Herein we deepen this research with experimental and computational methods by the investigation of the affinity of new rigid azaacene-based affinity materials (Figure 1a).[19–21] These were originally synthesized to investigate their optical and electronic behavior for the use in electro-organic devices such as organic solar cells. However, they feature unique structural moieties which are attractive for selective sensing. Decorating the phenylene-bridged core with sterically demanding alkyne-TIPS-protected azaacene moieties, a rigid structure results.[12,20,21] Rigidity and steric groups are shown by McKeown et al. to provide porous systems which are important for highly sensitive properties.[24] Additionally, the aromatic TIPS-protected azaacene moieties are critical; they facilitate hydrophobic interactions with aromatic analytes in a confined area and broadening the possible applicable analyte spectrum.

Results and Discussion

To determine the affinity of **Mo1**, **Mo2**, **Di1**, **Di2**, **Tr1**, **Tr2**, **Te1** and **Te2** (see Figure 1) towards different analytes, we used 195 MHz high-fundamental frequency QCMs (HFF-QCMs) with aluminum electrodes. A passivating perfluorinated layer was coated onto every QCM.[11] These passivated HFF-QCMs were further coated with the affinity materials via a reproducible electro-spray protocol, resulting in a well-controlled deposition of 10.4 ng (50 kHz of Δf).[11,25–28] This results in significantly higher surface-to-volume ratios of the affinity material, making close-surface cavities the predominant binding site for analytes.[18] These HFF-QCMs offer the advantage of superior detection limits and fast response times in comparison to QCMs with lower resonance frequency.[29] As analytes, we chose the BTX series (benzene, toluene and xylenes) and the more polar and precursors for illicit compounds acetone, GBL, phenylacetone, safrole and eugenol. The affinities were determined by passing a nitro-

gen stream enriched with a specific concentration of a given analyte over the QCMs at a controlled temperature of 35 °C. The analyte enrichment is performed at 20 °C to prevent condensation effects on the QCMs. The induced frequency shift Δf from the adsorbed analytes is measured precisely at multiply increased concentration levels. These frequency shifts can then be plotted against the respective concentration and fitted using the Langmuir equation and least-square nonlinear fitting, resulting in affinities for a material towards a given analyte.[30] For clarity, affinities were normalized to **Mo1**. Low analyte concentrations were chosen to focus on the study of specific binding sites. Further details about the QCM functionalization, the experimental set-up, the conditions, and the absolute data are available in the Supporting Information.

The chosen analytes belong to two groups: the less polar but aromatic analytes from the BTX series, which vary mainly in steric demand, and the more polar analytes, some of which are aromatic and others are not and they also vary in their steric and electronic properties. With these compounds, a wide range of interactions can be investigated.

Except for acetone and GBL, most analytes have aromatic moieties and are capable of aromatic interactions with the azaacene area, which is one of the predominant interactions in such cases. Especially, safrole and eugenol with their electron-rich aromatic systems may be well suited for electrostatic aromatic interactions with the electron-deficient azaacene moieties. Acetone and GBL will most likely rely on van der Waals interactions and CO–π or CO–H bonding. The measured affinities can be seen in Figure 1b. A clear trend is observed for all analytes between the smaller affinity materials such as the mono- and dimeric azaacenes **Mo1**, **Mo2**, **Di1** and **Di2** (green and gray) and the larger tri- and tetrameric azaacenes **Tr1**, **Tr2**, **Te1** and **Te2** (red and blue). The trimeric and tetrameric affinity materials exhibit affinities towards all of the measured analytes, which are at least twice as high when compared with those of the smaller derivatives. This might be due to the more bulky and rigid structure which leads to a higher porosity. This increased porosity, e.g., the comparison of **Tr2** to **Mo1**, can also be seen in the displayed surface-accessible surface area (SASA, approximation for the adsorption area) in Figure 1c. A higher porosity provides better accessibility for the analyte to the cavities of the material and therefore higher affinities. However, highly selective behavior could not be found towards the BTX series. **Tr1** and **Te1** both feature a smaller aromatic system and seem to be favorable for most members of the BTX series, except for *m*-xylene towards **Tr1**. This is due to size exclusion, as *m*-xylene is the sterically most demanding analyte in this case. We observe clear trends for the polar analytes. The low affinity for the monomeric and dimeric compounds continues with a mitigation in the case of phenylacetone. One reason could be the higher steric demand and additional dipole moment of the acetyl group compared to safrole or eugenol, which can lead to more unspecific adsorptions at less favorable binding sites. Despite having no aromatic systems, acetone and GBL still experience high affinities towards the trimeric and tetrameric systems. These analytes rely mostly on van der Waals interactions, CO–π or CO–H bonding. Additionally, due to their small size, they can efficiently use the more porous trimeric and tetrameric systems and access more restricted binding sites. The affinity of **Te1** towards GBL reached up to 32.9 Hz/ppm, which is the highest affinity known to date. In a previous work, the highest affinity of about 16.8 Hz/ppm was achieved by Pyka et al., which **Te1** exceeds by 96%, making it a highly interesting candidate for GBL sensing.[31] The analytes eugenol and safrole show anticipated high affinities towards the larger affinity materials, with a significant difference being **Tr2** and **Te2** experiencing higher affinities than the respective **Tr1** and **Te1**. Due to the sterically demanding propenyl and oxygen-containing groups, these analytes require more space to sufficiently undergo aromatic interactions, which is granted by the larger aromatic system present in **Te2** and **Tr2**. The affinity of **Tr2** towards safrole is elevated when compared to any other affinity material. It exhibits about five times higher affinity in comparison to **Mo1** and about 70% increased affinity when compared to **Te2**, the second highest affinity measured in this study. **Tr2** is uniquely sensitive towards safrole. Despite having similar electronic and steric properties, eugenol does not show similar trends to safrole, which might be explained by the higher steric demand of the methoxy group that could lead to impaired aromatic interaction capabilities. This kind of unique behavior of **Tr2** towards safrole was previously observed with a similar structure by Mastalerz et al. containing TIPS-alkyne protected azaacenes, connected by triptycene.[12] This indicates the importance of the TIPS-alkyne-protected azaacene, but also the significance of porosity caused by the trimeric core.

To understand the high selectivity towards safrole and GBL, we employed the xTB and xTB-IFF software by Grimme et al. in our computational study.[32–34] We collated the data available by single-crystal X-ray diffraction.[19–21] All quantum mechanical calculations were performed with xTB 6.4.1 and xTB-IFF 1.0.[32–34] Models of the SASA and binding sites were created with ChimeraX 1.3.[22,23] We took at least one unit cell of each affinity material and docked up to 50 analytes applying the intermolecular force field xTB-IFF. In each step the analyte is docked to 15 different positions within the structure, for which the single-point energies are calculated. The structure with the lowest energy is then chosen for further docking steps. The energies calculated represent the difference between the actual host–guest complex and the separate guest and previous host–guest complex energy. The obtained energies are then sorted and fitted, similar to the QCMs, and the resulting average interaction energy for all 50 adsorptions was normalized to **Mo1** and displayed in Figure 2b. As a direct comparison of the cal-

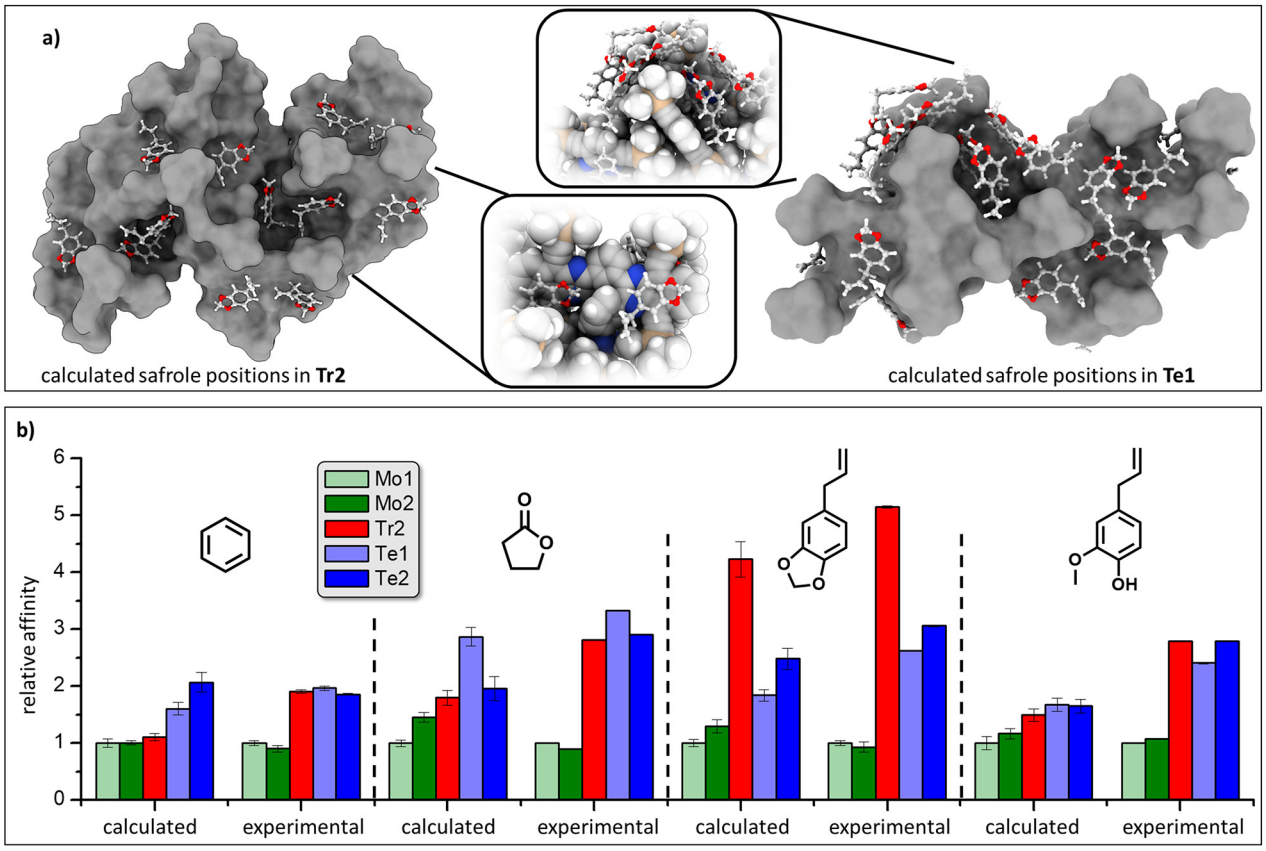

Figure 2 a) Display of the solvent-accessible surface area (SASA) of **Tr2** (left) and **Te1** (right). Display in these SASAs are the 25 most ideal binding sites for safrole calculated by xTB-IFF. b) Calculated relative affinities of the azaacenes **Mo1, Mo2, Tr2, Te1** and **Te2** towards the analytes benzene, GBL, safrole and eugenol. For better comparison, the experimental affinities are given alongside the calculated ones.

culated energies in kcal/mol and frequency shift in Hz/ppm is not possible, we compared the relative values to **Mo1**. The total and corrected energies can be found in the Supporting Information. The affinity materials **Tr2**, **Te1** and **Te2** were selected to be calculated as they exhibited the most promising affinities in the QCM measurements. Additionally, **Mo1** and **Mo2** were chosen as reference materials. As analytes, benzene, GBL, safrole and eugenol were chosen. The crystal structures were provided by the Bunz's group.[20,21] A crystal structure of **Tr1** could not be obtained and could therefore not be calculated. The use of crystal structures is an approximation to the QCM measurements, but with the use of these large systems we qualitatively simulate the possible guest–host interactions and obtain comparable results.

The calculated affinities, compared with the QCM-measured affinities, can be found in Figure 2b. Interestingly, the trend of low affinities for **Mo1** and **Mo2** can also be found for the calculated affinities, which is testament to the denser crystal structure with fewer cavities. In all cases, the elevated calculated affinities can be found for the bulkier affinity materials like **Tr2**, **Te1** and **Te2**. The calculated ratios are very close to QCM measurements in some cases, like **Te2** towards safrole with 1.9 calculated vs. 2.1 QCM-measured ratio to **Mo1**. In the case of benzene and eugenol, the calculated ratios for **Tr2** and **Te1** do not match the measured ratios and are significantly lower, but still higher than those for **Mo1** and **Mo2**. This might be due to effects and interactions that these calculations neglected, such as cooperative diffusion mechanisms.[35] For GBL, similar trends can be observed between the calculated and measured affinities. In the calculated results, **Te1** again exhibits very high affinities with obtained ratios of 2.9 for the calculations and 3.3 for the QCM measurements and confirms the choice of **Te1** to be used for possible sensing applications. In contrast to safrole, the calculated affinities of eugenol towards **Tr2** are not very high and even lower for **Te2** and **Te1**, which could also be explained by neglected interactions in the calculations. For safrole, the trends of the calculated affinities agree well with the measured affinities. The high affinity of **Tr2** towards safrole was confirmed with similar ratios of 4.23 cal-

culated and 5.15 measured. As this high selectivity is very interesting, we took a closer look at the calculated resulting structure (Figure 2a). The 25 best binding sites for safrole are displayed: towards **Tr2** (left) and **Te1** (right). Almost every safrole molecule on **Tr2** can be found at the location of an azaacene moiety, which confirms the importance of the aromatic binding sites. Furthermore, most of these binding sites are quite confined and incorporate the propenyl moiety of safrole – a key aspect to the high selectivity of **Tr2** towards safrole. In contrast, the binding sites at **Te1** (shown in Figure 2a, right side) show a less ideal behavior with very few interactions with the azaacene moiety, which might be due to the smaller size of the aromatic system.

Conclusions

The phenylene-bridged azaacene affinity materials were extensively investigated in their affinity and selectivity towards numerous gas-borne analytes utilizing QCM measurements and computational studies. These unique affinity materials showed attractive affinities and selectivities in QCM measurements. In particular, the high affinity of **Te1** towards GBL, which is the highest affinity found, opens new detection possibilities for this often abused compound.[3] An even higher selective behavior could be found with **Tr2** towards safrole, about 410% increased affinity compared to **Mo1**, which is the highest affinity increase measured with such materials. Therefore, **Tr2** could be used to create an efficient and portable sensor device, capable of detecting even traces of safrole – a precursor for the synthesis of amphetamines.[36] To investigate these affinity trends, further we employed the computational method xTB-IFF, which provided similar affinity trends to the QCM-measurements. The high affinity of **Te1** towards GBL was reproduced and confirmed. Additionally, the unique selectivity of **Tr2** towards safrole could also be calculated with these computational studies and confirmed our initial assumptions of the importance of aromatic interactions and confined binding sites. xTB-IFF is powerful in calculating the affinities of a given crystal structure, offering a tool to investigate cavities and binding sites in more detail. These insights might help in the future for better understanding of these unique selectivities and may assist in finding and designing new affinity materials.

Experimental Section

All commercially available chemicals were purchased from Sigma Aldrich or ABCR. QCM measurements were carried out using a previously described protocol.[31] Nitrogen used in the screening experiments has a purity of 99.998%. Reagents for the pretreatment of the QCMs: 1*H*,1*H*,2*H*,2*H*-perfluorooctyl-1-phosphonic acid (98%, ABCR, FP-8) in absolute ethanol.[11] The precoating of the passivating layer with FP-8 was performed with a concentration of 1.5 mmol/L in ethanol for 24 h and washing the QCMs several times with pure ethanol. HFF-QCMs with a fundamental frequency of 195 MHz were employed (*KVG Quartz Crystal Technology GmbH*, Neckarbischofsheim, Germany; type: XA 1600). The QCM is excited using an aperiodic oscillator circuit and oscillates with its specific load resonance frequency. Frequency counting is performed using a FPGA (field-programmable gate array) which allows asynchronous 28-bitcounting with an accuracy of ± 0.5 Hz.[13]

Procedures

Coating of QCMs: The coating of the QCMs is performed using an electrospray protocol.[25–27] This particular method is well established and allows the continuous monitoring of mass deposition onto the quartz during the spraying process. The electrospray solutions are prepared at concentrations of approximately 0.1 $mg \cdot mL^{-1}$ in a 9 : 1 mixture of tetrahydrofuran/methanol. The solution for coating is placed in a glass syringe (Hamilton, SYR 250 µL, 1725 RN) equipped with a metal cannula. The metallic needle is contacted with an applied voltage of 5 kV relative to a counter electrode, which is represented by the electrode of the QCM. A constant delivery of the solution during the coating process is achieved by using a syringe pump (Harvard Apparatus, Pump 11 Elite, 1 $\mu L \cdot min^{-1}$). The coating process is monitored by measuring the frequency shift of the QCM. All compounds are deposited on 195 MHz QCMs until a frequency shift of 50 kHz is reached. This shift corresponds to a mass of 10.4 ng of the deposited material on the oscillating QCM.

Measurement setup: For the determination of affinities, precise conditions and concentrations of analytes are required. For this setup, we used two mass flow controllers (MFCs) from the *Brooks Instrument company* (Model 5050S) both equipped with nitrogen. One of the flows generated by one of the MFCs is passed through an analyte reservoir which is adjusted to 293.1 ± 0.2 K. The analyte-saturated gas flow is mixed with the pure inert gas flow of the other MFC and is passed through the measuring chamber. The overall gas flow is set to 200 $mL \cdot min^{-1}$. By carefully controlling the flow of both streams by the MFCs, it is possible to produce gas mixtures with concentrations of 1% to 100% of the vapor pressure of the pure analyte at 293.1 ± 0.2 K. The central part of the screening setup is the measuring cell which is connected to the gas mixing unit and placed in a temperature-adjusted environment. We employed a slightly modified GC oven (*Hewlett Packard*, Palo Alto, California, United States; type: HP 5890). The cell is kept constant at 308 K to exclude temperature influences and to prevent con-

densation effects within the cell. The cell is designed to operate up to 12 QCMs in a parallel fashion.

Computational details: Into the unit cell cutouts of the affinity materials **Mo1**, **Mo2**, **Tr2**, **Te1** and **Te2**, four different analytes were docked (benzene, GBL, safrole and eugenol) up to 50 analytes, applying the intermolecular force field xTB-IFF. For these calculations, the computational tools xTB 6.4.1 and xTB-IFF 1.0 by Grimme et al. were used.[32–34] The obtained structures remained unoptimized, due to the size of the systems. The crystal structures were used as available at the Cambridge Crystallographic Data Centre.[20,21] For the visualization of molecules, ChimeraX 1.3 was used.[22,23] Parts of this research were conducted using the supercomputer Mogon and advisory services offered by Johannes Gutenberg University Mainz (hpc.uni-mainz.de), which is a member of the AHRP (Alliance for High Performance Computing in Rhineland Palatinate, www.ahrp.info) and the Gauss Alliance e.V.

More details on setup, QCM data and computational data can found in the Supporting Information.

Funding Information

U.H.F.B. thanks the DFG through the SFB 1249. Support by the Forschungsinitiative Rheinland-Pfalz in framing of SusInnoScience is highly appreciated.

Acknowledgment

The authors gratefully acknowledge the computing time granted on the supercomputer Mogon at Johannes Gutenberg University Mainz (hpc.uni-mainz.de).

Supporting Information

Supporting Information for this article is available online at https://doi.org/10.1055/a-1873-5186.

Conflict of Interest

The authors declare no conflict of interest.

References

(1) (a) Khan, F. I.; Kr. Ghoshal, A. *J. Loss Prev. Process Ind.* **2000**, *13*, 527. (b) Pinalli, R.; Pedrini, A.; Dalcanale, E. *Chem. Eur. J.* **2018**, *24*, 1010. (c) Lubczyk, D.; Hahma, A.; Brutschy, M.; Siering, C.; Waldvogel, S. R. *Propellants, Explos. Pyrotech.* **2015**, *40*, 590.
(2) Ryvlin, D.; Girschikofsky, M.; Schollmeyer, D.; Hellmann, R.; Waldvogel, S. R. *Global Challenges* **2018**, *2*, 1800057.
(3) Gimeno, P.; Besacier, F.; Bottex, M.; Dujourdy, L.; Chaudron-Thozet, H. *Forensic Sci. Int.* **2005**, *155*, 141.
(4) Brutschy, M.; Schneider, M. W.; Mastalerz, M.; Waldvogel, S. R. *Chem. Commun.* **2013**, *49*, 8398.
(5) (a) Baur, X.; Ollesch, T.; Poschadel, B.; Budnik, L. T.; Finger, S. Matz, G. *Zbl. Arbeitsmed.* **2007**, *57*, 89. (b) Zampolli, S.; Elmi, I.; Mancarella, F.; Betti, P.; Dalcanale, E.; Cardinali, G. C.; Severi, M. *Sens. Actuators, B* **2009**, *141*, 322. (c) Zampolli, S.; Betti, P.; Elmi, I.; Dalcanale, E. *Chem. Commun.* **2007**, *27*, 2790. (d) Clément, P.; Korom, S.; Struzzi, C.; Parra, E. J.; Bittencourt, C.; Ballester, P.; Llobet, E. *Adv. Funct. Mater.* **2015**, *25*, 4011. (e) Dickert, F. L.; Lieberzeit, P.; Miarecka, S. G.; Mann, K. J.; Hayden, O.; Palfinger, C. *Biosens. Bioelectron.* **2004**, *20*, 1040.
(6) Lynch, K. L. Mass Spectrometry for the Clinical Laboratory; Elsevier: Amsterdam, **2017**.
(7) (a) Wu, C.; Steiner, W. E.; Tornatore, P. S.; Matz, L. M.; Siems, W. F.; Atkinson, D. A.; Hill, H. H. *Talanta* **2002**, *57*, 123. (b) Mäkinen, M. A.; Anttalainen, O. A.; Sillanpää, M. E. T. *Anal. Chem.* **2010**, *82*, 9594.
(8) Oprea, A.; Weimar, U. *Anal. Bioanal. Chem.* **2019**, *411*, 1761.
(9) Oprea, A.; Weimar, U. *Anal. Bioanal. Chem.* **2020**, *412*, 6707.
(10) (a) Brutschy, M.; Schneider, M. W.; Mastalerz, M.; Waldvogel, S. R. *Adv. Mater.* **2012**, *24*, 6049. (b) Brutschy, M.; Stangenberg, R.; Beer, C.; Lubczyk, D.; Baumgarten, M.; Müllen, K.; Waldvogel, S. R. *ChemPlusChem* **2015**, *80*, 54. (c) Xu, T.; Xu, P.; Zheng, D.; Yu, H.; Li, X. *Anal. Chem.* **2016**, *88*, 12234. (d) Girschikofsky, M.; Rosenberger, M.; Belle, S.; Brutschy, M.; Waldvogel, S. R.; Hellmann, R. *Proc. SPIE–Int. Soc. Opt. Eng.* **2012**, *8439*, 843916. (e) Börner, S.; Orghici, R.; Waldvogel, S. R.; Willer, U.; Schade, W. *Appl. Opt.* **2009**, *48*, B183. (f) Orghici, R.; Willer, U.; Gierszewska, M.; Waldvogel, S. R.; Schade, W. *Appl. Phys. B* **2008**, *90*, 355. (g) Orghici, R.; Lützow, P.; Burgmeier, J.; Koch, J.; Heidrich, H.; Schade, W.; Welschoff, N.; Waldvogel, S. *Sensors* **2010**, *10*, 6788.
(11) Brutschy, M.; Lubczyk, D.; Müllen, K.; Waldvogel, S. R. *Anal. Chem.* **2013**, *85*, 10526.
(12) Prantl, E.; Kohl, B.; Ryvlin, D.; Biegger, P.; Wadepohl, H.; Rominger, F.; Bunz, U. H. F.; Mastalerz, M.; Waldvogel, S. R. *ChemPlusChem* **2019**, *13*, 1239.
(13) Wessels, A.; Klöckner, B.; Siering, C.; Waldvogel, S. R. *Sensors* **2013**, *13*, 12012.
(14) (a) Mujahid, A.; Afzal, A.; Dickert, F. L. *Sensors* **2019**, *19*, 4395. (b) Linke, A.; Jungbauer, S. H.; Huber, S. M.; Waldvogel, S. R. *Chem. Commun.* **2015**, *51*, 2040.
(15) (a) Lubczyk, D.; Siering, C.; Lörgen, J.; Shifrina, Z. B.; Müllen, K.; Waldvogel, S. R. *Sens. Actuators, B* **2010**, *143*, 561. (b) Lubczyk, D.; Grill, M.; Baumgarten, M.; Waldvogel, S. R.; Müllen, K. *ChemPlusChem* **2012**, *77*, 102.
(16) (a) Kohl, B.; Bohnwagner, M. V.; Rominger, F.; Wadepohl, H.; Dreuw, A.; Mastalerz, M. *Chem. Eur. J.* **2016**, *22*, 646. (b) Kohl, B.; Rominger, F.; Mastalerz, M. *Org. Lett.* **2014**, *16*, 704. (c) Kohl, B.; Rominger, F.; Mastalerz, M. *Chem. Eur. J.* **2015**, *21*, 17308.
(17) Dickert, F. L.; Bäumler, U. P. A.; Stathopulos, H. *Anal. Chem.* **1997**, *69*, 1000.
(18) Schaub, T. A.; Prantl, E. A.; Kohn, J.; Bursch, M.; Marshall, C. R.; Leonhardt, E. J.; Lovell, T. C.; Zakharov, L. N.; Brozek, C. K.; Waldvogel, S. R.; Grimme, S.; Jasti, R. *J. Am. Chem. Soc.* **2020**, *142*, 8763.
(19) Bunz, U. H. F.; Freudenberg, J. *Acc. Chem. Res.* **2019**, *52*, 1575.
(20) Hahn, S.; Alrayyani, M.; Sontheim, A.; Wang, X.; Rominger, F.; Miljanić, O. Š.; Bunz, U. H. F. *Chem. Eur. J.* **2017**, *23*, 10543.
(21) Hahn, S.; Koser, S.; Hodecker, M.; Seete, P.; Rominger, F.; Miljanić, O. Š.; Dreuw, A.; Bunz, U. H. F. *Chem. Eur. J.* **2018**, *24*, 6968.

(22) Goddard, T. D.; Huang, C. C.; Meng, E. C.; Pettersen, E. F.; Couch, G. S.; Morris, J. H.; Ferrin, T. E. *Protein Sci.* **2018**, *27*, 14.
(23) Pettersen, E. F.; Goddard, T. D.; Huang, C. C.; Meng, E. C.; Couch, G. S.; Croll, T. I.; Morris, J. H.; Ferrin, T. E. *Protein Sci.* **2021**, *30*, 70.
(24) (a) Abbott, L. J.; McKeown, N. B.; Colina, C. M. *J. Mater. Chem. A* **2013**, *1*, 11950. (b) Abbott, L. J.; McDermott, A. G.; Del Regno, A.; Taylor, R. G. D.; Bezzu, C. G.; Msayib, K. J.; McKeown, N. B.; Siperstein, F. R.; Runt, J.; Colina, C. M. *J. Phys. Chem. B* **2013**, *117*, 355. (c) Taylor, R. G. D.; Bezzu, C. G.; Carta, M.; Msayib, K. J.; Walker, J.; Short, R.; Kariuki, B. M.; McKeown, N. B. *Chem. Eur. J.* **2016**, *22*, 2466.
(25) Fenn, J. B. *Angew. Chem. Int. Ed. Engl.* **2003**, *42*, 3871.
(26) Fenn, J. B. *Angew. Chem.* **2003**, *115*, 3999.
(27) Heil, C.; Windscheif, G.; Braschohs, S.; Flörke, J.; Gläser, J.; Lopez, M.; Müller-Albrecht, J.; Schramm, U.; Bargon, J.; Vögtle, F. *Sens. Actuators, B* **1999**, *61*, 51.
(28) Wortmann, A.; Kistler-Momotova, A.; Zenobi, R.; Heine, M. C.; Wilhelm, O.; Pratsinis, S. E. *J. Am. Soc. Mass Spectrom.* **2007**, *18*, 385.
(29) Neubig, B.; Briese, W. Das große Quarzkochbuch. Quarze, Quarzoszillatoren, Quarz- und Oberflächenwellenfilter (SAW), Meßtechnik; Franzis: Feldkirchen, **1997**.
(30) Masel, R. I. Principles of Adsorption and Reaction on Solid Surfaces; Wiley: New York, **1996**.
(31) Pyka, I.; Ryvlin, D.; Waldvogel, S. R. *ChemPlusChem* **2016**, *81*, 926.
(32) Bannwarth, C.; Ehlert, S.; Grimme, S. *J. Chem. Theory Comput.* **2019**, *15*, 1652.
(33) Grimme, S.; Bannwarth, C.; Caldeweyher, E.; Pisarek, J.; Hansen, A. *J. Chem. Phys.* **2017**, *147*, 161708.
(34) Grimme, S.; Bannwarth, C.; Shushkov, P. *J. Chem. Theory Comput.* **2017**, *13*, 1989.
(35) Atwood, J. L.; Barbour, L. J.; Jerga, A.; Schottel, B. L. *Science* **2002**, *298*, 1000.
(36) Swist, M.; Wilamowski, J.; Parczewski, A. *Forensic Sci. Int.* **2005**, *155*, 100.